Vibrational spectra and structures of Si$_n$C clusters (n = 3–8)†

Nguyen Xuan Truong,[a] Marco Savoca,[a] Dan J. Harding,[bc] André Fielicke[a] and Otto Dopfer*[a]

The effects of doping bare silicon clusters with carbon on their physical properties are of fundamental interest for the chemistry of the interstellar medium and the development of novel nanostructures in materials science. Carbon-doped silicon clusters (Si$_n$C, n = 3–8) are characterized in the gas phase with infrared-ultraviolet two-color ionization (IR-UV2CI) spectroscopy, mass spectrometry, and quantum chemical calculations. Structural identification is achieved by comparing the measured and calculated vibrational absorption spectra of the low-energy Si$_n$C isomers identified by global optimization algorithms. Except for planar Si$_3$C, the most stable Si$_n$C clusters have three-dimensional configurations. While the Si$_3$C and Si$_6$C structures are uniquely assigned, several stable isomers of Si$_4$C, Si$_5$C, Si$_7$C, and Si$_8$C may co-exist under the present experimental conditions. Interestingly, some of the structures observed here are different from the ground state structures predicted previously. For the small neutral clusters (n ≤ 5), structures similar to those reported previously for the anions are observed. The highly stable Si$_3$C unit with a nearly linear Si–C–Si motif is identified as characteristic building block in several of the most stable Si$_n$C structures. In all identified structures, a large negative charge of almost −2e is located on the C atom, indicating its role as electron donor in the Si$_n$ host moiety. The B3LYP/cc-pVTZ level proves reliable in finding the experimentally observed isomers.

I. Introduction

Silicon–carbon based nanotubes, nanowires, and clusters are of great interest as promising building blocks for the synthesis of novel materials at the nanoscale.[1] In addition, small silicon–carbon clusters, *e.g.*, SiC$_m$ with m = 1–4, were found in interstellar space.[2–7] Hence understanding the nature of Si–C bonding might, on the one hand, open a way toward engineering of such nanostructures at the atomic level. On the other hand, it is crucial for several chemical processes and observations in the interstellar medium.[8–11] Although located in the same main group of the periodic table, silicon and carbon exhibit very different physical and chemical properties. Silicon prefers multi-directional single bonds, while carbon can easily form single, double, and triple bonds. Generally, substituting a single Si atom with a C atom in a pure Si$_n$ cluster induces strong distortions, but the geometric topology maintains.[12,13] When doped into

silicon clusters, the C atom favors locations with more than threefold coordinated bonding in the ground state structures, making most Si$_n$C$_m$ clusters more stable than their pure silicon counterparts.[13]

There have been numerous theoretical studies on silicon–carbon clusters.[13–33] For small-sized clusters, for example, the ground state structures and vibrational spectra of Si$_3$C and Si$_2$C$_3$ were determined using Hartree–Fock (HF) and second-order many body perturbation (MP2) theories.[14,15] A clear trend of favorable geometries in the transition from pure carbon to pure silicon clusters was observed, *i.e.*, the chain-like carbon-rich and three-dimensional silicon-rich clusters. This has also been observed for Si$_n$C$_m$ (n + m ≤ 8) cluster anions in both theory[32] and experiments.[12] Most close to our work, two lowest-energy Si$_4$C structures were found at the CCSD(T) level, *i.e.*, the minimum trigonal C_{3v} pyramid and a distorted edge capped C_{2v} pyramid (about 21 kJ mol^{-1} higher).[33] At the HF level, however, the latter structure lies about 8 kJ mol^{-1} lower than the former. Additional calculations of infrared (IR) spectra, isotopic shifts, and dipole moments indeed hinted at their coexistence.[33]

In contrast to theory, spectroscopic characterization of silicon–carbon clusters is largely lacking. Most previous studies have concentrated on charged clusters isolated in the gas phase or neutrals in an inert matrix. For instance, photoelectron (PE) spectra of Si$_n$C$_m$$^-$ (1 ≤ n ≤ 7, 1 ≤ m ≤ 5) cluster anions found

a Institut für Optik und Atomare Physik, Technische Universität Berlin, Hardenbergstraße 36, D-10623 Berlin, Germany. E-mail: dopfer@physik.tu-berlin.de

b Institut für Physikalische Chemie, Georg-August-Universität Göttingen, Tammannstraße 6, D-37077 Göttingen, Germany

c Department of Dynamics at Surfaces, Max-Planck-Institut für Biophysikalische Chemie, Am Faßberg 11, D-37077 Göttingen, Germany

† Electronic supplementary information (ESI) available. See DOI: 10.1039/c5cp02588e

This journal is © the Owner Societies 2015

Phys. Chem. Chem. Phys., 2015, **17**, 18961–18970 | **18961**

that Si_nC^- ($3 \leq n \leq 7$) and their Si_{n+1}^- counterparts have a similar topology.[12] The PE spectrum of SiC_3^- shows electronic transitions, corresponding to both linear and cyclic forms.[34] However, no conclusion about the true global minimum on the SiC_3 potential energy surface could be drawn. With Fourier-transform infrared spectroscopy in Ar matrices combined with quantum chemical calculations, the molecular structures of small Si_nC_m ($n + m \leq 5$) clusters were determined, e.g., a linear centrosymmetric geometry for Si_2C_3 and a rhomboidal C_{2v} structure for Si_3C.[35–38] Furthermore, Si_3C_2 is a pentagon, and Si_2C_4 has a linear symmetric geometry in the ground state.[39] Similarly, C-rich clusters such as SiC_4, SiC_5, SiC_7, and SiC_9, were found to exhibit chain-like structures.[38,40–43] For small Si_nC_m clusters with $n + m \leq 4$, the electronic structure has been studied by resonant photoionization.[11,44,45] In general, little spectroscopic information is available for somewhat larger Si-rich Si_nC_m clusters, which is the topic of the present work.

Through recent advances in the generation of intense IR laser radiation, novel spectroscopic methods for neutral clusters in the gas phase have been developed, such as IRMPD (infrared multiple photon dissociation),[46,47] IR-REMPI (infrared resonance enhanced multiple photon ionization),[48] and IR-UV2CI (infrared-ultraviolet two-color ionization).[49] While IR-REMPI spectra are often broadened due to the absorption of several hundred IR photons, the IR-UV2CI spectra can be better resolved and more closely related to the linear IR absorption spectra. Employing the IR-UV2CI technique for neutral Si_nC_m clusters, we recently observed the evolution from 3D to 1D chain-like configurations in Si_nC_{6-n} clusters by sequentially substituting Si with C atoms in pure Si_6.[50] In addition, the influence of first-row dopant atoms on the properties of bare silicon clusters (Si_6X with X = Be, B, C, N, O) has been determined.[51] As expected, the geometric and electronic properties of silicon containing clusters can substantially be modified by changing the dopant atom.

Here we identify the geometric and electronic structures of Si_nC clusters with n = 3–8 via their IR-UV2CI spectra. Combining quantum chemical calculations with global optimization,[52,53] the low-energy Si_nC isomers are determined. Structural identification is achieved through comparison of the measured IR-UV2CI spectra with the IR spectra predicted for the corresponding low-energy isomers. Results for Si_5C and Si_6C have been reported elsewhere,[50,51] but are included here with additional insights for completeness. Electronic properties and charge distributions of selected low-energy isomers will also be discussed.

II. Experimental and computational methods

The IR-UV2CI setup has been described elsewhere.[47,49,50] Briefly, carbon-doped silicon clusters are produced by laser ablation of a pure silicon rod within a pulsed flow of He gas containing 1% CH_4 and thermalized to about 100 K in a liquid-nitrogen cooled expansion channel. After passing through a skimmer, the neutral Si_nC_m clusters are overlapped with counter-propagating IR radiation from the 'Free Electron Laser for Infrared eXperiments' (FELIX)[54]

and then post-ionized by an unfocused F_2 laser (E_{F_2} = 7.87 eV) in the extraction zone of a reflectron time-of-flight mass spectrometer. For clusters of specific sizes, with an ionization energy (IE) close to E_{F_2}, prior resonant excitation with IR photons from a FELIX pulse raises the internal energy and thereby enhances the efficiency for ionization by the UV laser pulse that is about 30 μs delayed. Resonant excitation of a vibrational mode is followed by rapid internal vibrational energy redistribution, leading to complete thermalization on this experimental timescale. The ionization efficiency usually follows a S-curve behavior as a function of excitation energy, with a slope depending on the Franck–Condon factor for ionization. An increase of the internal energy of the cluster upon IR absorption therefore results in an enhancement of the ionization yield and its IR wavelength dependence closely reflects the linear vibrational absorption spectrum of the neutral cluster. The IR-UV2CI spectra in Fig. 1 are obtained from the relative ionization enhancement normalized by the IR photon flux.[55] The observed widths of the bands of 15–45 cm^{-1} arise from a combination of unresolved rotational
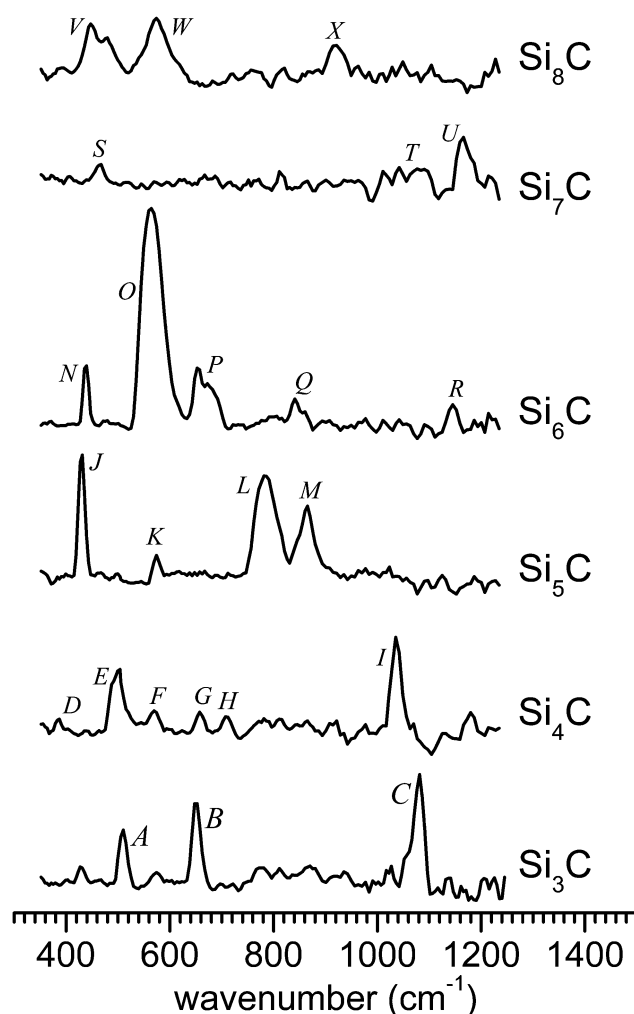

Fig. 1 Measured IR-UV2CI spectra of Si_nC (with n = 3–8). All spectra are drawn to the same scale, according to the relative IR enhancement normalized by laser fluence.

18962 | Phys. Chem. Chem. Phys., 2015, 17, 18961–18970

This journal is © the Owner Societies 2015

structure, sequence hot band transitions involving low-frequency modes, the FELIX bandwidth (*ca.* 0.5–1% full width at half maximum (FWHM) of the central wavelength), and possibly the multiple photon absorption process.

Quantum chemical calculations are performed for both singlet and triplet states of each cluster. In an effort to thoroughly explore the complex potential energy surface of the cluster, we employ global optimization (GO) techniques such as the genetic (GA) and basin hopping (BH) algorithms.[56,57] Details of our BH implementation have been given elsewhere.[51,52] Basically, there are two major steps. First, up to five thousand candidate structures are evaluated in terms of the total energy by the GO coupled with DFT calculations at the RI-BP86/def-SVP level as implemented in TURBOMOLE V6.3.1.[58] Second, the first twenty nonequivalent lowest-energy isomers are tightly re-optimized at the B3LYP/cc-pVTZ level including the Grimme dispersion correction (D3)[59] with the resolution-of-the-identity approximation as implemented in GAUSSIAN09.[60] At this level, the linear IR absorption spectra, ionization and binding energies, and natural bond orbital (NBO) populations are obtained. To facilitate convenient comparison with the experimental spectra, the theoretical IR absorption stick spectra are convoluted with a 20 cm^{-1} FWHM Gaussian profile. The reported vibrational frequencies are unscaled. Similar calculations for selected clusters have been performed at the TPSS/cc-pVTZ and MP2/cc-pVTZ levels, which have also proven reliable for doped Si clusters.[47,49,50] The vertical electronic transitions of selected Si_nC clusters are calculated at the second-order approximate coupled cluster RI-CC2/def2-TZVP and TD-DFT/cc-pVTZ levels using TURBOMOLE V6.3.1.[58] As the excited-state calculation for high-symmetry structures (*e.g.*, C_{3v}, C_{4v}, and C_{5v}) is not supported at the CC2 level, the C_1 point group is used for these clusters.

III. Results and discussion

The IR-UV2CI spectra measured for Si_nC (n = 3–8), the linear IR absorption spectra and the geometries of the respective lowest-energy isomers calculated at the B3LYP/cc-pTVZ level are shown in Fig. 1–7. The computational spectra are all drawn to the same linear intensity scale for direct comparison. The relative energies, ionization and binding energies are listed in Tables 1 and 2, respectively. Vertical excitations (Table 3) of selected Si_nC isomers are also provided. Natural bond orbital charges, vibrational and geometric data of all structures considered are available in Tables 1–3 in the ESI.† In the following discussion, the optimized structures obtained at the B3LYP level are used if not stated otherwise.

A. Vibrational spectra and geometries

Si_3C. The experimental IR-UV2CI spectrum of Si_3C is compared in Fig. 2 with the linear absorption spectra calculated for the first three lowest-energy isomers **3a**–**3c**. Three bands are observed at 509 (A), 651 (B), and 1080 cm^{-1} (C), which can readily be explained with structure **3a**. In the investigated spectral range (350–1250 cm^{-1}), **3a** exhibits significant absorptions at 509 (a_1), 652 (a_1), and 1109 cm^{-1} (b_2), arising from the Si–C–Si symmetric stretching mode, the symmetric breathing mode, and the Si–C–Si asymmetric stretching mode, respectively. Our results are consistent with previous work based on Ar-matrix Fourier-transform IR spectroscopy combined with *ab initio* calculations[37] and excited-state measurements.[44,45] In the former, five of the six vibrational fundamental frequencies (in cm^{-1}) were determined as 309.5 (a_1), 357.6 (b_2), 511.8 (a_1), 658.2 (a_1), and 1101.4 (b_2). The shifts from the IR-UC2CI data are rather small and may be related to matrix effects and/or the multiphotonic IR excitation in the gas-phase experiments.

Structure **3a** has been predicted as the ground state of Si_3C.[13,14,22,61,62] While the ground state of neutral Si_4 has a D_{2h} (^1A_g) rhomboidal geometry,[63–65] **3a** is a distorted rhombus (C_{2v}, $^1A_1$) with shorter and stronger C–Si bonds and a nearly linear Si–C–Si bridge ($\angle 4Si–1C–2Si = 164.9°$). The calculated C–Si bond lengths of 1.764 and 1.944 Å are close to the previous results.[44] The anion counterpart Si_3C^- has been concluded to be a distorted planar rhombus (C_{2v}, $^2A_2$), due to the similarity

Table 1 Relative energies (in kJ mol^{-1}) of the most stable Si_nC (n = 3–8) isomers calculated at the B3LYP, TPSS, and MP2 levels using the cc-pVTZ basis set

Cluster	Isomer	Symmetry (State)	Relative energy			Cluster	Isomer	Symmetry (State)	Relative energy		
			B3LYP	TPSS	MP2				B3LYP	TPSS	MP2
Si_3C	**3a**	C_{2v} ($^1A_1$)	**0.0**	**0.0**	**0.0**	Si_6C	**6a**	C_{5v} ($^1A_1$)	**0.0**	**0.0**	**0.0**
	3b	C_{2v} ($^3B_1$)	116.6	117.1	187.0		**6b**	C_s ($^1A'$)	12.2	36.8	86.5
	3c	C_s ($^3A''$)	183.1	157.8^a	199.0		**6c**	C_1 (^1A)	29.3	56.1	105.5
							6d	C_s ($^1A'$)	47.2	59.9	86.5
Si_4C	**4a**	C_2 (^1A)	**0.0**	19.9	24.2	Si_7C	**7a**	C_1 (^1A)	**0.0**	7.2	21.0
	4b	C_{3v} ($^1A_1$)	1.1	**0.0**	**0.0**		**7b**	C_1 (^1A)	0.2	6.0	29.2
	4c	C_s ($^1A'$)	18.7	38.3	28.9^b		**7c**	C_{3v} ($^1A_1$)	9.9	8.8	31.2
	4d	C_s ($^1A'$)	27.9	52.9	55.0		**7d**	C_s ($^1A'$)	14.4	**0.0**	**0.0**
						Si_8C	**8a**	C_s ($^1A'$)	**0.0**	**0.0**	64.6
Si_5C	**5a**	C_{2v} ($^1A_1$)	**0.0**	→**5b**	→**5b**		**8b**	C_1 (^1A)	3.1	7.1	**0.0**
	5b	C_{4v} ($^1A_1$)	0.1	**0.0**	**0.0**		**8c**	C_1 (^1A)	17.6	13.8	54.4
	5c	C_s ($^1A'$)	33.2	44.1	76.5		**8d**	C_s ($^1A'$)	22.1	10.6	**0.0**
	5d	C_s ($^3A''$)	123.4	133.9	197.2		**8e**	C_s ($^1A'$)	39.8	18.0	49.7

^{a} Relaxing to a (C_{3v}, $^3A_1$) structure. ^{b} C_{2v} ($^1A_1$).

Table 2 Vertical ionization energy (VIE), adiabatic ionization energy (AIE), and averaged binding energy (BE) of the low-energy Si_nC isomers calculated at the B3LYP, TPSS, and MP2 levels using the cc-pVTZ basis set (separated by semicolons, left to right, respectively)

Cluster	Isomer	VIE [eV]	AIE [eV]	BE [eV]
Si_3C	3a	8.13; 8.21; 8.43	7.80; 8.00; 8.12	4.90; 5.14; 5.25
	3b	6.71; 6.89; 6.42	6.64; 6.83; 6.18	4.60; 4.83; 4.76
	3c	7.16; 7.48; 7.10	5.91; 6.43; 6.06	4.43; 4.73; 4.73
Si_4C	4a	7.90; 8.02; 8.54	7.30; 7.46; 7.44	4.75; 5.06; 5.15
	4b	8.15; 8.25; 8.72	7.94; 8.11; 8.37	4.75; 5.10; 5.20
	4c	7.46; 7.60; 7.77	7.10; 7.27; 7.39	4.71; 5.02; 5.14
	4d	7.32; 7.45; 7.64	7.17; 7.31; 7.50	4.69; 4.99; 5.08
Si_5C	5a	8.19; 8.27; 8.72	7.83; 7.93; 8.61	4.86; 5.26; 5.48
	5b	8.19; 8.21; 8.72	7.95; 7.98; 8.61	4.86; 5.26; 5.48
	5c	8.00; 8.03; 8.74	7.62; 7.67; #	4.81; 5.19; 5.35
	5d	7.51; 7.48; 8.69	6.62; 6.54; #	4.65; 5.03; 5.14
Si_6C	6a	7.85; 7.85; 8.16	7.56; 7.69; 8.16	4.73; 5.17; 5.40
	6b	8.00; 7.78; 8.00	7.70; 7.33; 7.36	4.72; 5.12; 5.28
	6c	7.18; 7.58; 7.80	7.04; 7.13; 7.17	4.69; 5.09; 5.25
	6d	7.42; 7.44; 7.68	7.05; 7.10; 7.41	4.66; 5.08; 5.28
Si_7C	7a	7.59; 7.66; 8.18	7.32; 7.38; #	4.69; 5.09; 5.27
	7b	7.60; 7.65; 8.17	7.31; 7.39; 7.91	4.69; 5.09; 5.26
	7c	7.81; 7.84; 8.40	7.41; 7.43; 7.76	4.68; 5.09; 5.25
	7d	7.52; 7.53; 8.06	7.07; 7.13; 7.45	4.67; 5.10; 5.30
Si_8C	8a	7.52; 7.63; 8.24	7.12; 7.33; 7.73	4.69; 5.12; 5.29
	8b	7.75; 7.73; 8.23	7.48; 7.49; #	4.69; 5.11; 5.37
	8c	7.47; 7.44; 8.49	7.24; 7.25; #	4.67; 5.10; 5.30
	8d	7.47; 7.48; 8.23	7.24; 7.28; 8.08	4.66; 5.11; 5.37
	8e	7.41; 7.42; 7.67	7.18; 7.24; 7.37	4.64; 5.10; 5.31

calculations failed to converge.

Table 3 Vertical excitations of selected Si_nC (n = 3–8) isomers calculated at the RI-CC2/def2-TZVP and B3LYP/cc-pVTZ levels[a]

Cluster	Isomer (point group, state)	Transition energy [eV]	
		RI-CC2/def2-TZVP	B3LYP/cc-pVTZ
Si_3C	3a (C_{2v}, $^1A_1$)	2.08 ($^1B_2$, 3.21)	1.87 ($^1B_2$, 1.54)
		2.83 ($^1A_2$, 0.00)	3.08 ($^1B_2$, 27.82)
		3.09 ($^1A_2$, 0.00)	3.77 ($^1B_2$, 17.18)
Si_4C	4a (C_2, ^1A)	2.25 (^1B, 17.7)	2.20 (^1B, 10.39)
		2.49 (^1A, 8.65)	2.39 (^1B, 8.03)
		2.63 (^1B, 4.19)	2.40 (^1A, 5.54)
	4b (C_{3v}, $^1A_1$)	2.77 (^1A, 10.6)	2.57 ($^1A_1$, 2.62)
		2.79 (^1A, 0.00)	2.63 (^1E, 38.28)
		2.83 (^1A, 1.56)	3.19 (^1E, 12.43)
Si_5C	5a (C_{2v}, $^1A_1$)	3.40 ($^1A_2$, 0.00)	3.17 ($^1A_1$, 0.15)
		3.51 ($^1A_2$, 0.00)	3.28 ($^1A_1$, 0.18)
		3.57 ($^1A_1$, 0.00)	3.42 ($^1B_2$, 0.03)
	5b (C_{4v}, $^1A_1$)	3.38 (^1A, 0.00)	3.18 (^1A, 0.24)
		3.49 (^1A, 0.00)	3.49 (^1E, 2.65)
		3.55 (^1A, 0.00)	3.77 (^1E, 26.42)
Si_6C	6a (C_{5v}, $^1A_1$)	2.59 (^1A, 0.00)	3.26 ($^1E_1$, 23.87)
		3.47 (^1A, 0.00)	3.44 ($^1A_1$, 12.62)
		3.51 (^1A, 10.17)	3.56 ($^1E_1$, 2.80)
Si_7C	7a (C_1, ^1A)	2.03 (^1A, 2.01)	2.22 (^1A, 0.77)
		2.24 (^1A, 0.34)	2.39 (^1A, 0.67)
		2.43 (^1A, 0.39)	2.49 (^1A, 1.36)
	7b (C_1, ^1A)	2.38 (^1A, 0.81)	2.42 (^1A, 0.66)
		2.52 (^1A, 0.35)	2.59 (^1A, 0.41)
		2.68 (^1A, 1.91)	2.68 (^1A, 0.71)
	7c (C_{3v}, $^1A_1$)	2.09 (^1A, 0.36)	1.94 (^1E, 0.05)
		2.48 (^1A, 0.00)	2.43 (^1E, 0.56)
		2.50 (^1A, 0.07)	2.78 (^1E, 1.08)
Si_8C	8a (C_s, $^1A'$)	2.19 ($^1A'$, 1.38)	1.99 ($^1A'$, 0.37)
		2.28 ($^1A''$, 14.69)	2.17 ($^1A''$, 0.10)
		2.55 ($^1A'$, 11.90)	2.34 ($^1A''$, 2.40)
	8b (C_1, ^1A)	2.15 (^1A, 0.00)	2.12 (^1A, 0.53)
		2.32 (^1A, 2.29)	2.24 (^1A, 2.86)
		2.51 (^1A, 8.64)	2.47 (^1A, 1.71)
	8c (C_1, ^1A)	1.65 (^1A, 0.54)	2.07 (^1A, 2.34)
		2.08 (^1A, 2.91)	2.29 (^1A, 4.29)
		2.14 (^1A, 2.83)	2.42 (^1A, 1.22)

[a] For structures 4b (C_{3v}), 5b (C_{4v}), and 6a (C_{5v}), calculations with C_1 symmetry are performed at the RI-CC2 level. Numbers in parentheses are the oscillator strengths in 10^{-3}.

between the PE spectra of Si_3C^- and Si_4^-.[11,12,61] The good agreement observed between the measured and predicted frequencies of Si_3C in Fig. 2 supports the use of the B3LYP/cc-pVTZ level for the structural and vibrational assignment of the larger carbon-doped silicon clusters described below. The next two stable isomers 3b (C_{2v}, $^3B_1$) and 3c (C_s, $^3A''$) are triplet states with relative energies well above 100 kJ mol^{-1} (Fig. 2). Isomer 3b exhibits a planar Y-shaped geometry, while 3c is a distorted triangular pyramid. At the MP2 level, isomer 3c relaxes to a C_{3v} ($^3A_1$) distorted tetrahedron.

Si_4C. Fig. 3 compares the measured IR-UV2CI spectrum of Si_4C with linear IR spectra predicted for the four lowest-energy isomers 4a–4d. Six distinct bands are observed at 388 (D), 499 (E), 571 (F), 659 (G), 710 (H), and 1037 cm^{-1} (I). Except for band F, all features can be explained with the fundamental modes of the two most stable isomers 4a and 4b. Specifically, bands D and E are assigned to Si–C–Si bending modes of 4a predicted at 378 (a) and 490 cm^{-1} (a), while band I is attributed to the asymmetric stretching of the nearly linear 4Si–1C–5Si moiety (176.8°) at 1047 cm^{-1} (b). Bands G and H with similar peak intensities are assigned to the breathing mode at 660 cm^{-1} (a_1) and the asymmetric Si–C stretching mode at 721 cm^{-1} (e) of isomer 4b. In addition, the breathing mode at 395 cm^{-1} (a_1) of 4b fits well to band D with a small redshift of about 10 cm^{-1}.

Interestingly, isomer 4b (C_{3v}, $^1A_1$) is often predicted as the ground state structure of Si_4C,[12,13,61,64] as also obtained here

with the TPSS and MP2 methods (Table 1). This structure is formed by replacing the Si atom at one of the apexes of the trigonal bipyramidal Si_5 (D_{3h}, $^1A_1'$) cluster.[66] However, the energy difference between 4a and 4b is known to be strongly dependent on the theoretical level.[33] For example, the present B3LYP calculations predict a lower-symmetry ground state structure 4a (C_2, ^1A), and the next stable structures are 1.1 (4b), 18.7 (4c, C_s, $^1A'$), and 27.9 kJ mol^{-1} (4d, C_s, $^1A'$) higher in energy. Structure 4a with an estimated IE of about 7.9 eV (Table 2) is expected to yield a somewhat different IR-UVC2I enhancement than 4b with a slightly higher IE (8.15 eV). Nonetheless, the observed relative band intensities in Fig. 3 suggest that the population of both isomers are of similar order of magnitude. The ground state structure of Si_4C (4a) is similar to the most stable structure of its anion counterpart Si_4C^- (C_{2v}, $^2A_1$) predicted at the MP2/6-31G* level.[12,61] A significant contribution of

18964 | *Phys. Chem. Chem. Phys.*, 2015, **17**, 18961–18970

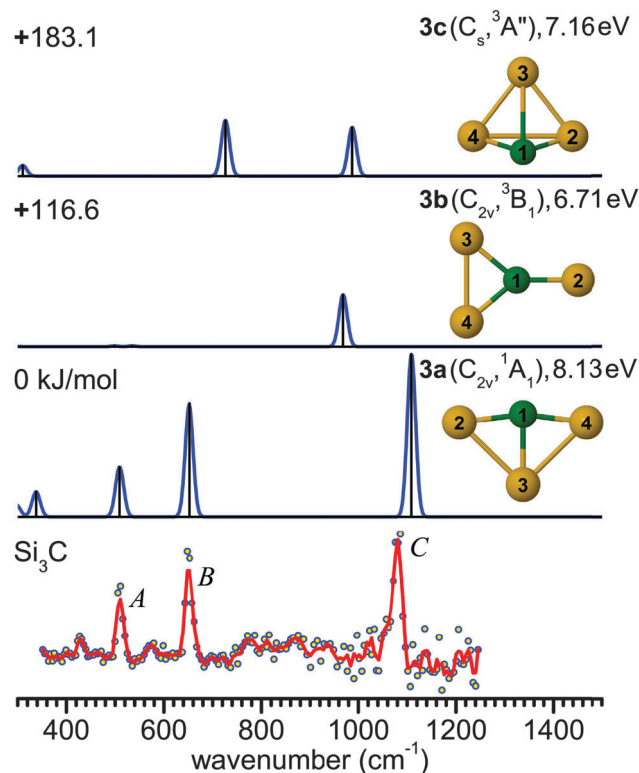This journal is © the Owner Societies 2015

Fig. 2 Comparison of the experimental IR-UV2CI spectrum of Si$_3$C (bottom) with linear IR spectra of the three lowest-energy isomers (**3a–3c**) calculated at the B3LYP/cc-pVTZ level. Molecular symmetries and electronic states are given in parentheses, while vertical ionization energies are given in eV. Relative energies are given in kJ mol^{-1}. The red line is the three-point adjacent average of the original data (circles). The experimental peak positions (in cm^{-1}) are 509 (A), 651 (B) and 1080 (C).
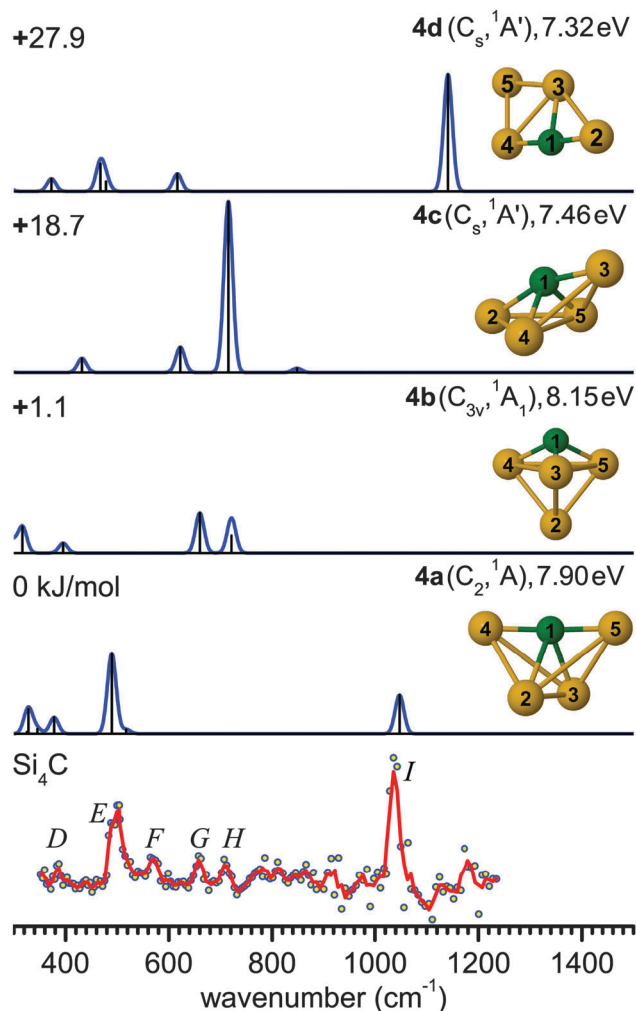
Fig. 3 Comparison of the experimental IR-UV2CI spectrum of Si$_4$C (bottom) with linear vibrational spectra of the four lowest-energy isomers (**4a–4d**) calculated at the B3LYP/cc-pVTZ level. Molecular symmetries and electronic states are given in parentheses. Relative energies are given in kJ mol^{-1}, while vertical ionization energies are given in eV. The red line is the three-point adjacent average of the original data (circles). The experimental peak positions (in cm^{-1}) are 388 (D), 499 (E), 571 (F), 659 (G), 710 (H), and 1037 (I).

4c and **4d** to the IR-UV2CI spectrum is ruled out, because of their substantially higher energies and the mismatch of their predicted IR spectrum with the measured one. Finally, we note that the Si$_4$C structures assigned from the IR-UV2CI spectrum are different from those postulated from the analysis of the photodetachment experiments of the corresponding anions.[61] This example illustrates the importance of the direct spectroscopic study of the neutral clusters for the reliable experimental determination of the true ground state.

Si$_5$C. The experimental IR-UV2CI spectrum of Si$_5$C[50] is compared in Fig. 4 to the linear IR spectra of the four lowest-energy isomers (**5a–5d**). Four bands are observed at 427 (J), 573 (K), 785 (L), and 868 cm^{-1} (M), which are mostly related to structures **5a/b**. The ground state structure of Si$_5$C has widely been predicted as a distorted tetragonal bipyramid **5b** (C_{4v}, $^1A_1$), which has a similar geometry as the corresponding Si$_6$ (D_{4h}, $^1A_{1g}$) cluster.[65–67] This scenario is also supported by our TPSS and MP2 calculations (Table 1), and the IR-UV2CI spectrum has indeed been assigned to **5b** in our previous study by the comparison with the calculated TPSS spectrum.[50] The bands J, K, and L, agree well with the predicted fundamentals, while band M has been explained with the overtone of J,[50] although its intensity is surprisingly high for an overtone.

The B3LYP/cc-pVTZ level suggests an alternative scenario. In contrast to the MP2 and TPSS levels, B3LYP yields a ground state structure **5a** (C_{2v}, $^1A_1$) resulting from a distortion of the C_{4v} cage **5b**, along with an energy lowering of only 0.1 kJ mol^{-1}, while **5b** is a low-lying transition state, leading to a fluxional structure. Similar to **5a**, the low frequency bands J and K can again be assigned to deformation and breathing modes at 424 (a$_1$) and 565 cm^{-1} (a$_1$). While in the higher frequency range, the **5b** spectrum shows a single intense degenerate peak at 785 cm^{-1} (e) in excellent agreement with band L, **5a** exhibits two split vibrational modes at 726 cm^{-1} (b$_1$, asymmetric Si–C stretching of 4Si–1C–6Si) and 847 cm^{-1} (b$_2$, asymmetric Si–C stretching of 3Si–1C–5Si). These may be assigned to bands L and M, however with unusually large redshifts of up to 50 cm^{-1} from experiment, which possibly arise from unusual anharmonicity along the distortion coordinate.

Similar findings were noted for isovalent Si$_6$.[47,49] Two possible ground state structures have also been proposed for Si$_6$ showing
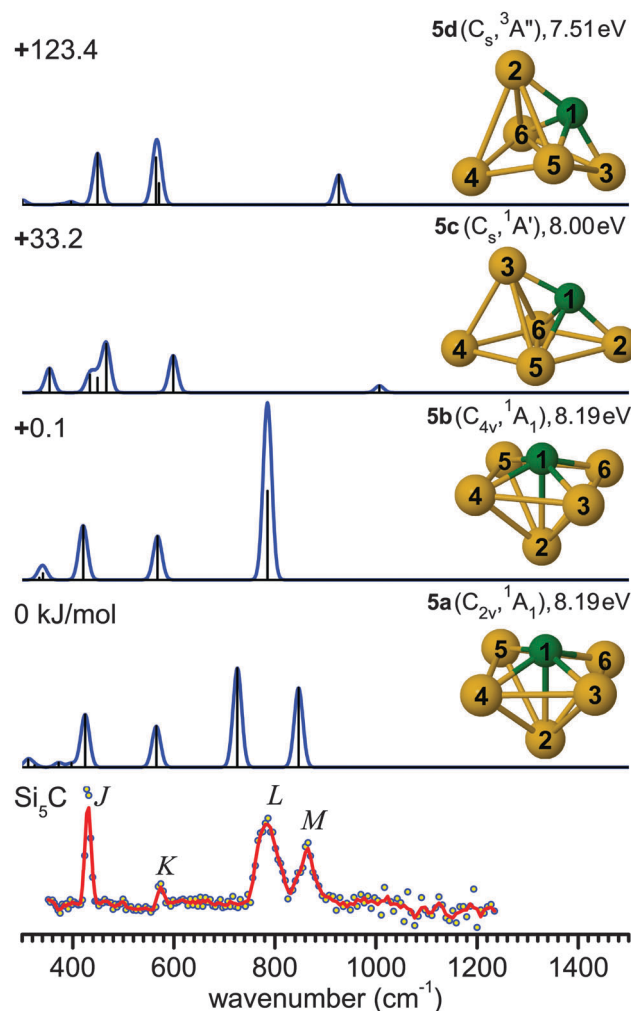
This journal is © the Owner Societies 2015

Phys. Chem. Chem. Phys., 2015, **17**, 18961–18970 | **18965**

Fig. 4 Comparison of the experimental IR-UV2CI spectrum of Si_5C (bottom)[50] with linear vibrational spectra of the four lowest-energy isomers (**5a–5d**) calculated at the B3LYP/cc-pVTZ level. Molecular symmetries and electronic states are given in parentheses, while vertical ionization energies are given in eV. Relative energies are given in kJ mol^{-1}. The red line is the three-point adjacent average of the original data (circles). The experimental peak positions (in cm^{-1}) are 430 (J), 574 (K), 786 (L), and 863 (M).
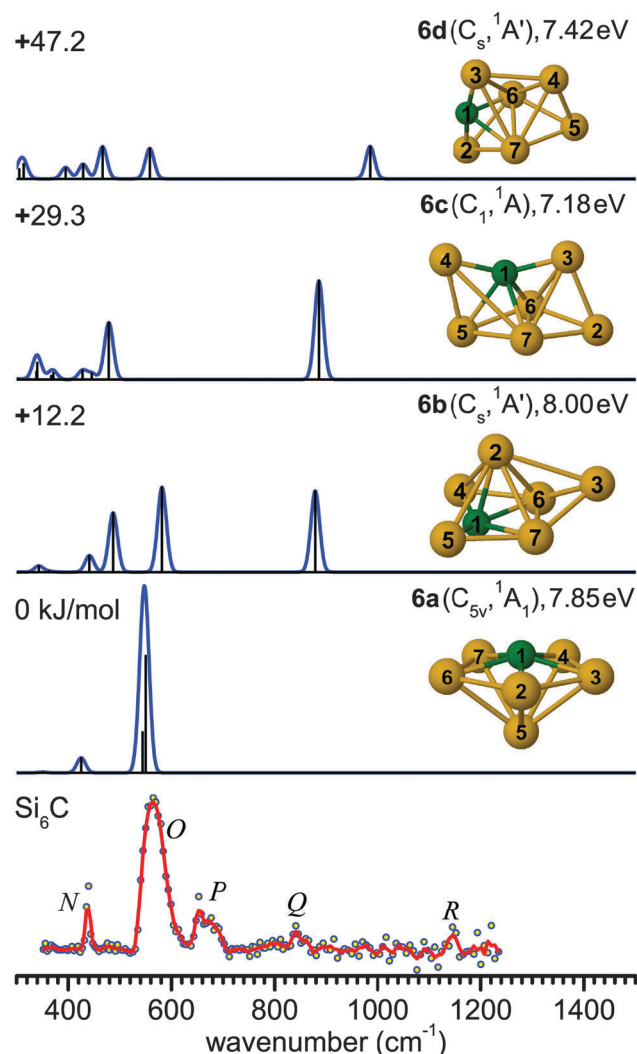

Fig. 5 Comparison of the experimental IR-UV2CI spectrum of Si_6C (bottom) with linear vibrational spectra of the four lowest-energy isomers (**6a–6d**) calculated at the B3LYP/cc-pVTZ level. Molecular symmetries and electronic states are given in parentheses. Relative energies are given in kJ mol^{-1}, while vertical ionization energies are given in eV. The red line is the three-point adjacent average of the original data (circles). The experimental peak positions (in cm^{-1}) are 438 (N), 566 (O), 664 (P), 842 (Q), and 1137 (R).

the best agreement with the measured IR-UV2CI spectra, *i.e.*, a C_{2v} ($^1A_1$) structure found by DFT and a D_{4h} ($^1A_{1g}$) structure predicted with MP2. This difference has been reasoned as distortions in Si_6 induced by a pseudo Jahn–Teller effect.[67,68] It was impossible to draw a firm conclusion on the true ground state structure of Si_6, as a potential band splitting for the C_{2v} structure was unresolved experimentally. For Si_5C, the splitting is larger ($\sim$120 cm^{-1}) and hence observable. More theoretical efforts need to be devoted to the pseudo Jahn–Teller effects in Si_6 and Si_5C to fully understand the measured IR spectra. Such efforts are, however, beyond the scope of the present work.

For comparison, quantum chemical calculations for Si_5C^- have indicated a C_{2v} ($^2A_1$) ground state for the anion, but the PE spectrum has been interpreted to mainly originate from a C_s ($^2A'$) anion into a C_s ($^1A'$) neutral state (corresponding to **5c**).[12,61] Similar to Si_4C, the structures of the neutral Si_5C

clusters derived from the IR and PE spectra are different, due to the vertical transitions favored by the Franck–Condon principle.

Si_6C. The results for Si_6C published recently[51] are included here for completeness. Fig. 5 compares the IR-UV2CI spectrum of Si_6C with linear IR spectra of the four lowest-energy isomers (**6a–6d**). Five bands are detected at 438 (N), 566 (O), 664 (P), 842 (Q) and 1137 cm^{-1} (R). All these features can readily be explained by structure **6a** (C_{5v}, $^1A_1$) with the C atom at the apex of a pentagonal bipyramid, which has widely been accepted as the ground state structure of Si_6C.[13,22,32,51] Its shape is similar to the D_{5h} ($^1A_1'$) ground state of Si_7 determined in experiments[49,66,69] and theory.[63,66,70] Band N is assigned to the breathing mode at 425 cm^{-1} (a_1), while band O is assigned to the asymmetric and

symmetric Si–C stretching modes at 544 cm^{-1} (e$_1$) and 550 cm^{-1} (a$_1$), respectively. A fundamental mode near 660 cm^{-1} (P) is not predicted for any of the low-energy isomers. Therefore, we tentatively assign it to a combination band of the a$_1$ mode predicted at 425 cm^{-1} with the low frequency modes at 226 (e$_1$) or 257 cm^{-1} (a$_1$). Similarly, the weaker band Q might be an overtone of the mode at 425 cm^{-1} (a$_1$), and band R may be related to an overtone and/or combination of the modes at 544 cm^{-1} (e$_1$) and 550 cm^{-1} (a$_1$).

Si$_7$C. The IR-UV2CI spectrum of Si$_7$C and the linear absorption spectra and geometries of the four lowest-energy isomers (**7a–7d**) are displayed in Fig. 6. Three bands are observed at 464 (S), 1075 (T), and 1163 cm^{-1} (U). The two intense bands S and U can be explained with structure **7b** (C$_1$, ^{1}A), which at the

Fig. 6 Comparison of the experimental IR-UV2CI spectrum of Si$_7$C (bottom) with linear vibrational spectra of the four lowest-energy isomers (**7a–7d**) calculated at the B3LYP/cc-pVTZ level. Molecular symmetries and electronic states are given in parentheses. Relative energies are given in kJ mol^{-1}, while vertical ionization energies are given in eV. The red line is the three-point adjacent average of the original data (circles). The experimental peak positions (in cm^{-1}) are 464 (S), 1075 (T) and 1163 (U). Arrows indicate weak bands at 678 and 769 cm^{-1}, which might be attributed to the modes at 679 (**7a**) and 768 cm^{-1} (**7c**), respectively.

B3LYP level is slightly higher in energy (0.2 kJ mol^{-1}) than the most stable one, **7a** (C$_1$, ^{1}A). Band S is assigned to the Si–C–Si bending mode at 461 cm^{-1} (a), while band U is attributed to the asymmetric Si–C–Si stretching mode at 1195 cm^{-1} (a). Although structures **7a** and **7c** (C$_{3v}$, ^{1}A$_1$) also exhibit IR active modes close to band S, neither of their intense bands at 680 (**7a**) and 768 cm^{-1} (**7c**) is observed in the experiment. We therefore exclude their substantial contribution to the observed spectrum. Actually, closer inspection of Fig. 6 reveals that the small signal at 678 cm^{-1} marked by an arrow may be attributed to **7a**. Indeed, band T fits well to the asymmetric Si–C–Si stretching mode of **7a** calculated at 1103 cm^{-1} (a). Similar to **3a** and **4a**, the Si–C stretching modes at high frequency are characterized by the nearly linear Si–C–Si motifs present in **7a** (∠ 5Si–1C–3Si = 175.8°) and **7b** (∠ 4Si–1C–3Si = 168.4°). Interestingly, while **7d** (C$_s$, ^{1}A′) has been predicted as the ground state structure of Si$_7$C (see ref. 22 and 32 and our TPSS and MP2 calculations), no signal of its most intense stretching mode at 526 cm^{-1} (a″) is observed in the IR-UV2CI spectrum. This structure is obtained by substituting a Si atom by a C atom in a deformed bicapped Si$_8$ octahedron (C$_{2h}$, ^{1}A$_g$).[47,70,71] We note that the relative energies of the four considered isomers **7a–7d** are quite small (<15 kJ mol^{-1} at the B3LYP and TPSS levels, Table 1). Their calculated IE values (7.5–7.8 eV, Table 2) are relatively low compared to the photon energy of the F$_2$ laser. This may strongly affect the possibilities of detecting substantial enhancements in the ionization yield upon resonant IR absorption.[47]

Si$_8$C. The experimental IR-UV2CI spectrum of Si$_8$C and the calculated linear IR spectra of the five lowest-energy isomers **8a–8e** are compared in Fig. 7. The present B3LYP and TPSS calculations predict **8a** (C$_s$, ^{1}A′) as the most stable structure, which is in agreement with previous work.[13] Structure **8a** is analogous to its Si$_9$ counterpart (C$_s$, ^{1}A′).[47,70] Other stable isomers (**8b–8e**) higher in energy have similar topological geometries. The IR-UV2CI spectrum of Si$_8$C shows three major bands at 449 (V), 574 (W), and 922 cm^{-1} (X). These features can readily be explained with isomer **8b**, which is only 1.3 kJ mol^{-1} above the putative global minimum **8a**. Specifically, band V and W are assigned to Si–C–Si bending modes at 452 cm^{-1} (a) and 563 cm^{-1} (a), respectively. Band X is attributed to the asymmetric Si–C–Si stretching mode at 962 cm^{-1} (a) of the almost linear Si–C–Si unit (∠ 7Si–1C–6Si = 160°).

The main feature in the IR spectrum of isomer **8a** at 446 (a′) coincides with band V. Interestingly, structure **8a** also contains the linear Si–C–Si block with ∠ 4Si–1C–2Si = 179.5°. The corresponding asymmetric Si–C–Si stretching mode at 1051.7 cm^{-1} (a′) is, however, weak. Therefore, a contribution of this isomer to the measured spectrum cannot be ruled out from the calculated IR spectrum. However, its calculated IE value is rather low (7.52 eV), so that the IR-UV2CI enhancement using 7.87 eV photons is probably weak. Similar conclusions apply to all higher energy isomers (7.41–7.47 eV for **8c–8e**) with the notable exception of the identified isomer **8b** (7.75 eV). Hence, our favored assignment of the measured spectrum is mainly to isomer **8b**, while the presence of further isomers in the beam cannot be excluded. No other experimental information about Si$_8$C is available for comparison.
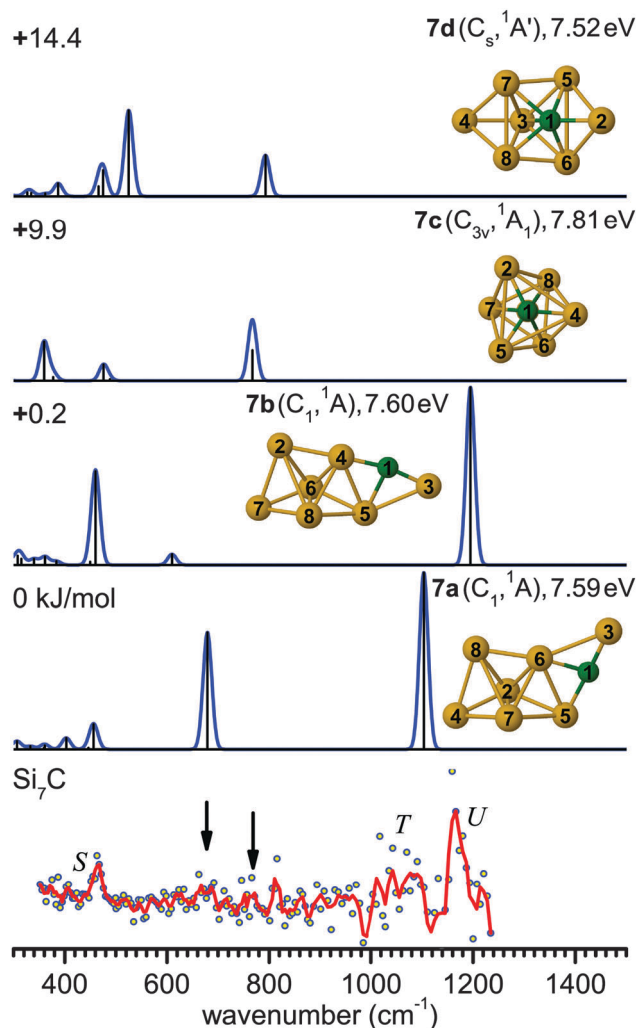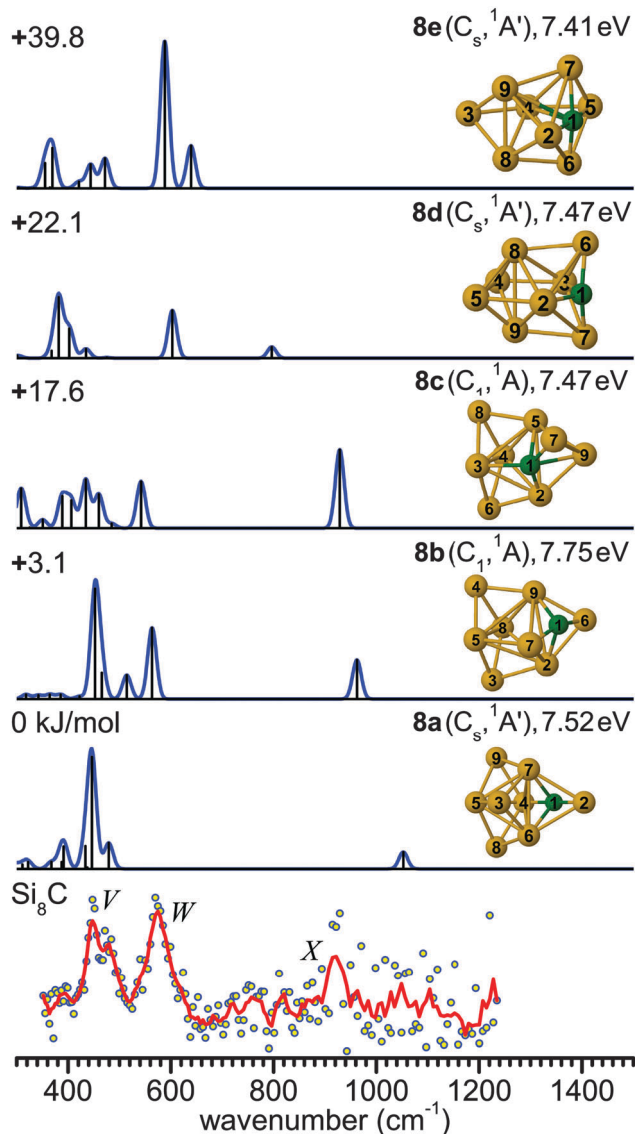
Fig. 7 Comparison of the experimental IR-UV2CI spectrum of Si₈C (bottom) with linear vibrational spectra of the five lowest-energy isomers (**8a–8e**) calculated at the B3LYP/cc-pVTZ level. Molecular symmetries and electronic states are given in parentheses. Relative energies are given in kJ mol^{-1}, while vertical ionization energies are given in eV. The red line is the three-point adjacent average of the original data (circles). The experimental peak positions (in cm^{-1}) are 449 (V), 574 (W), and 922 (X).

B. Structural and electronic properties

The evolution of structures with increasing size for Si$_n$C (n = 3–8) is summarized in the left part of Fig. 8 showing the isomers that explain the major features of the experimental spectra. Most of these structures contain a Si$_3$C substructure with a (nearly) linear Si–Si unit, except Si$_5$C and Si$_6$C. Interestingly, the Si$_3$C cluster (along with Si$_2$C) has been identified as a particular stable size in fragmentation experiments.[72,73] This stability, thermodynamically and as structural element, may be explained in terms of its valence structure as shown in Fig. 8 (right). Boys localization of the eight valence orbitals reveals the presence of three lone pairs, each at one of the Si
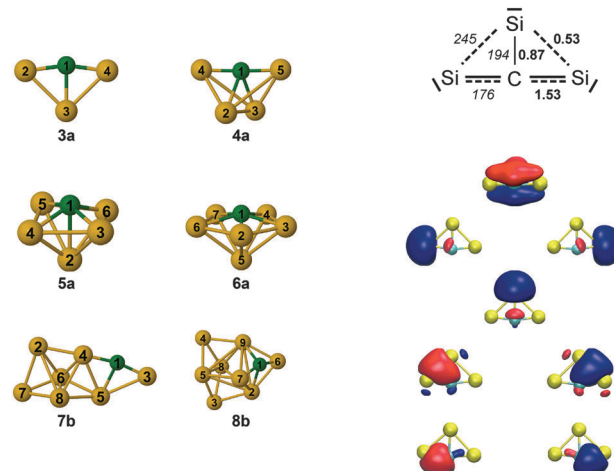

Fig. 8 (left) Overview of the structures observed for Si$_n$C (n = 3–8). Most of these structures contain a Si$_3$C substructure with a (nearly) linear Si–C–Si unit, except Si$_5$C and Si$_6$C. (right) Valence structure and localized molecular orbitals for Si$_3$C as obtained from a Boys localization. Formal bond orders (bold) are compared to the bond lengths in pm (italics).

atoms, two Si–C σ-bonds in the Si–C–Si unit, as well as three delocalized bonds, one of them being a π-bond delocalized over the entire cluster. The resulting formal bond orders range from 0.53 between neighboring Si atoms to 1.53 within the linear Si–C–Si unit. The high bond order in the Si–C–Si unit goes along with relatively short Si–C bond lengths of 176 pm as compared to the third Si–C bond, which is 194 pm long and has a formal bond order of only 0.87. The larger clusters also have similar bond lengths within the Si–C–Si bridge unit. The average of the corresponding Si–C distances in this unit is a measure of its strength and can be directly related with the frequency of the asymmetric Si–C–Si stretching mode observed experimentally. For the structures in which we identify this element (**3a, 4a, 7b, 8b**) this particular mode is found at 1080, 1037, 1163 and 922 cm^{-1}, respectively, and the average Si–C distances are 176, 178, 174 and 183 pm, i.e. there is a clear anti-correlation between bond length and stretching frequency.

The NBO charge analysis is increasingly used for a view of local charge instead of the unreliable Mulliken population analysis. As expected for Si$_n$C clusters, a large negative charge is located at the C atom (almost $-2e$, Table S1 in ESI†), which is more electronegative than Si. The positive part is mainly shared by the Si atoms directly bound to the C atom. This result suggests that these Si atoms are very good electron donors, as observed previously for the first-row element doped silicon clusters.[51]

Vertical excitations of selected stable clusters calculated with the second-order approximate coupled cluster and TD-DFT methods are listed in Table 3 for the first three transitions. The first electronic transition energies for the considered clusters are relatively high ($>$1.65 eV).

IV. Conclusions

Carbon-doped silicon clusters are characterized with IR-UV2CI spectroscopy combined with quantum chemical simulations.

18968 | Phys. Chem. Chem. Phys., 2015, 17, 18961–18970

This journal is © the Owner Societies 2015

The structures of the Si$_n$C (n = 3–8) clusters are determined by comparison of the measured IR-UV2CI spectra with linear IR absorption spectra of the low-energy isomers calculated at the B3LYP/cc-pVTZ level. Optimized stable structures are found employing global optimization algorithms coupled with electronic structure (DFT) methods. This technique is robust and reliable in searching for the ground state structures of such type of clusters, in which electronic effects might play an important role. For Si$_3$C and Si$_6$C, only the lowest-energy isomers are present in the prepared cluster sample, while for Si$_4$C, Si$_5$C, Si$_7$C, and Si$_8$C multiple stable structures may co-exist. The nearly linear motif (Si–C–Si) is identified as characteristic building block in several of the most stable Si$_n$C structures (n = 3–5, 7, 8). The NBO analysis shows that most charge is located on the C atom and its nearest-neighbor Si atoms. Although the theoretical approaches used in this work agree well on predicting low-energy isomers, the B3LYP method proves to be the most reliable one in finding the ground state structures.

Acknowledgements

References

1 P. Melinon, B. Masenelli, F. Tournus and A. Perez, *Nat. Mater.*, 2007, **6**, 479–490.

2 I. Cherchneff, Y. H. Le Teuff, P. M. Williams and A. G. G. M. Tielens, *Astron. Astrophys.*, 2000, **357**, 572–580.

3 K. P. Lim and F. W. Lampe, *Int. J. Mass Spectrom.*, 1990, **101**, 245–256.

4 S. K. Mandal and H. W. Roesky, *Chem. Commun.*, 2010, **46**, 6016–6041.

5 D. S. N. Parker, A. V. Wilson, R. I. Kaiser, N. J. Mayhall, M. Head-Gordon and A. G. G. M. Tielens, *Astrophys. J*, 2013, **770**, 33.

6 P. Thaddeus, S. E. Cummins and R. A. Linke, *Astrophys. J.*, 1984, **283**, L45–L48.

7 M. Frenklach, C. S. Carmer and E. D. Feigelson, *Nature*, 1989, **339**, 196–198.

8 F. Combes, M. Boquien, C. Kramer, E. M. Xilouris, F. Bertoldi, J. Braine, C. Buchbender, D. Calzetti, P. Gratier, F. Israel, B. Koribalski, S. Lord, G. Quintana-Lacaci, M. Relano, M. Rollig, G. Stacey, F. S. Tabatabaei, R. P. J. Tilanus, F. van der Tak, P. van der Werf and S. Verley, *Astron. Astrophys.*, 2012, **539**, A67.

9 K. Furuya, Y. Aikawa, K. Tomida, T. Matsumoto, K. Saigo, K. Tomisaka, F. Hersant and V. Wakelam, *Astrophys. J.*, 2012, **758**, 86.

10 M. Satta, T. Grassi and F. A. Gianturco, *Mon. Not. R. Astron. Soc.*, 2013, **429**, 269–274.

11 M. Steglich and J. P. Maier, *Astrophys. J.*, 2015, **801**, 119.

12 A. Nakajima, T. Taguwa, K. Nakao, M. Gomei, R. Kishi, S. Iwata and K. Kaya, *J. Chem. Phys.*, 1995, **103**, 2050.

13 Q. Y. Chu, B. X. Li and J. Yu, *J. Mol. Struct.*, 2007, **806**, 67–76.

14 C. M. L. Rittby, *J. Chem. Phys.*, 1992, **96**, 6768–6772.

15 C. M. L. Rittby, *J. Chem. Phys.*, 1994, **100**, 175–180.

16 R. S. Grev and H. F. Schaefer, *J. Chem. Phys.*, 1984, **80**, 3552–3555.

17 R. S. Grev and H. F. Schaefer, *J. Chem. Phys.*, 1985, **82**, 4126–4130.

18 R. S. Grev and H. F. Schaefer, *Chem. Phys. Lett.*, 1985, **119**, 111–118.

19 I. L. Alberts, R. S. Grev and H. F. Schaefer, *J. Chem. Phys.*, 1990, **93**, 5046–5052.

20 Z. Y. Jiang, X. H. Xu, H. S. Wu, F. Q. Zhang and Z. H. Jin, *J. Mol. Struct.*, 2002, **589**, 103–109.

21 Z. Y. Jiang, X. H. Xu, H. S. Wu, F. Q. Zhang and Z. H. Jin, *Chin. J. Struct. Chem.*, 2003, **22**, 459–463.

22 Z. Y. Jiang, X. H. Xu, H. S. Wu and Z. H. Jin, *J. Phys. Chem. A*, 2003, **107**, 10126–10131.

23 Z. Y. Jiang, X. H. Xu, H. S. Wu, F. Q. Zhang and Z. H. Jin, *Chem. Phys.*, 2003, **290**, 223–231.

24 Z. Y. Jiang, X. H. Xu, H. S. Wu, F. Q. Zhang and Z. H. Jin, *J. Mol. Struct.*, 2003, **624**, 61–67.

25 Z. Y. Jiang, X. H. Xu, H. S. Wu, F. Q. Zhang and Z. H. Jin, *J. Mol. Struct.*, 2003, **621**, 279–284.

26 J. Hou and B. Song, *J. Chem. Phys.*, 2008, **128**, 154304.

27 B. Song, Y. Yong, J. Hou and P. He, *Eur. Phys. J. D*, 2010, **59**, 399–406.

28 J. Zhang, W. C. Lu, Q. J. Zang, L. Z. Zhao, C. Z. Wang and K. M. Ho, *J. Phys.: Condens. Matter*, 2011, **23**, 205305.

29 S. Erkoc and L. Turker, *Physica E*, 2000, **8**, 50–56.

30 M. Cui, M. Ge, J. Feng, H. Zhang, W. Tian and C. Sun, *J. Mol. Struct.*, 1999, **492**, 241–256.

31 Q. X. Li, W. C. Lu, Q. J. Zang, L. Z. Zhao, C. Z. Wang and K. M. Ho, *Comput. Theor. Chem.*, 2011, **963**, 439–447.

32 S. Hunsicker and R. O. Jones, *J. Chem. Phys.*, 1996, **105**, 5048–5060.

33 A. D. Zdetsis, G. Froudakis, M. Muhlhauser and H. Thumnel, *J. Chem. Phys.*, 1996, **104**, 2566–2573.

34 G. E. Davico, R. L. Schwartz and W. C. Lineberger, *J. Chem. Phys.*, 2001, **115**, 1789–1794.

35 J. D. Presilla-Marquez, S. C. Gay, C. M. L. Rittby and W. R. M. Graham, *J. Chem. Phys.*, 1995, **102**, 6354–6361.

36 J. D. Presilla-Marquez and W. R. M. Graham, *J. Chem. Phys.*, 1994, **100**, 181–185.

37 J. D. Presilla-Marquez and W. R. M. Graham, *J. Chem. Phys.*, 1992, **96**, 6509–6514.

38 P. A. Withey and W. R. M. Graham, *J. Chem. Phys.*, 1992, **96**, 4068–4072.

39 J. D. Presilla-Marquez, C. M. L. Rittby and W. R. M. Graham, *J. Chem. Phys.*, 1996, **104**, 2818–2824.

This journal is © the Owner Societies 2015

Phys. Chem. Chem. Phys., 2015, **17**, 18961–18970 | 18969

40 T. H. Le, C. M. L. Rittby and W. R. M. Graham, *J. Chem. Phys.*, 2014, **140**, 064314.

41 X. D. Ding, S. L. Wang, C. M. L. Rittby and W. R. M. Graham, *J. Phys. Chem. A*, 2000, **104**, 3712–3717.

42 X. D. Ding, S. L. Wang, C. M. L. Rittby and W. R. M. Graham, *J. Chem. Phys.*, 1999, **110**, 11214–11220.

43 J. D. Presilla-Marquez, C. M. L. Rittby and W. R. M. Graham, *J. Chem. Phys.*, 1997, **106**, 8367–8373.

44 N. J. Reilly, M. Steglich, D. L. Kokkin, J. P. Maier, J. F. Stanton and M. C. McCarthy, *J. Mol. Spectrosc.*, 2015, **310**, 135–140.

45 J. F. Stanton, J. Dudek, P. Theule, H. Gupta, M. C. McCarthy and P. Thaddeus, *J. Chem. Phys.*, 2005, **122**, 124314.

46 P. Gruene, D. M. Rayner, B. Redlich, A. F. G. van der Meer, J. T. Lyon, G. Meijer and A. Fielicke, *Science*, 2008, **321**, 674–676.

47 M. Haertelt, J. T. Lyon, P. Claes, J. de Haeck, P. Lievens and A. Fielicke, *J. Chem. Phys.*, 2012, **136**, 064301.

48 G. von Helden, D. van Heijnsbergen and G. Meijer, *J. Phys. Chem. A*, 2003, **107**, 1671–1688.

49 A. Fielicke, J. T. Lyon, M. Haertelt, G. Meijer, P. Claes, J. de Haeck and P. Lievens, *J. Chem. Phys.*, 2009, **131**, 171105.

50 M. Savoca, A. Lagutschenkov, J. Langer, D. J. Harding, A. Fielicke and O. Dopfer, *J. Phys. Chem. A*, 2013, **117**, 1158–1163.

51 N. X. Truong, M. Savoca, D. J. Harding, A. Fielicke and O. Dopfer, *Phys. Chem. Chem. Phys.*, 2014, **16**, 22364–22372.

52 D. J. Harding, C. Kerpal, G. Meijer and A. Fielicke, *J. Phys. Chem. Lett.*, 2013, **4**, 892–896.

53 R. Gehrke and K. Reuter, *Phys. Rev. B: Condens. Matter Mater. Phys.*, 2009, **79**, 085412.

54 D. Oepts, A. F. G. van der Meer and P. W. van Amersfoort, *Infrared Phys. Technol.*, 1995, **36**, 297–308.

55 M. Haertelt, A. Fielicke, G. Meijer, K. Kwapien, M. Sierka and J. Sauer, *Phys. Chem. Chem. Phys.*, 2012, **14**, 2849–2856.

56 S. Heiles and R. L. Johnston, *Int. J. Quantum Chem.*, 2013, **113**, 2091–2109.

57 D. J. Wales, *Energy landscapes*, Cambridge University Press, Cambridge, 2003.

58 E. M. Fernández, J. M. Soler, I. L. Garzón and L. C. Balbás, *Phys. Rev. B: Condens. Matter Mater. Phys.*, 2004, **70**, 165403.

59 S. Grimme, J. Antony, S. Ehrlich and H. Krieg, *J. Chem. Phys.*, 2010, **132**, 154104.

60 M. J. Frisch, G. W. Trucks, H. B. Schlegel, G. E. Scuseria, M. A. Robb, J. R. Cheeseman, G. Scalmani, V. Barone, B. Mennucci, G. A. Petersson, H. Nakatsuji, M. Caricato, X. Li, H. P. Hratchian, A. F. Izmaylov, J. Bloino, G. Zheng, J. L. Sonnenberg, M. Hada, M. Ehara, K. Toyota, R. Fukuda, J. Hasegawa, M. Ishida, T. Nakajima, Y. Honda, O. Kitao, H. Nakai, T. Vreven, J. A. Montgomery Jr, J. E. Peralta, F. Ogliaro, M. Bearpark, J. J. Heyd, E. Brothers, K. N. Kudin, V. N. Staroverov, R. Kobayashi, J. Normand, K. Raghavachari, A. Rendell, J. C. Burant, S. S. Iyengar, J. Tomasi, M. Cossi, N. Rega, N. J. Millam, M. Klene, J. E. Knox, J. B. Cross, V. Bakken, C. Adamo, J. Jaramillo, R. Gomperts, R. E. Stratmann, O. Yazyev, A. J. Austin, R. Cammi, C. Pomelli, J. W. Ochterski, R. L. Martin, K. Morokuma, V. G. Zakrzewski, G. A. Voth, P. Salvador, J. J. Dannenberg, S. Dapprich, A. D. Daniels, Ö. Farkas, J. B. Foresman, J. V. Ortiz, J. Cioslowski and D. J. Fox, *GAUSSIAN09, Rev.D.01*, Gaussian Inc., Wallingford CT, 2009.

61 R. Kishi, M. Gomei, A. Nakajima, S. Iwata and K. Kaya, *J. Chem. Phys.*, 1996, **104**, 8593–8604.

62 P. S. Yadav, R. K. Yadav, S. Agrawal and B. K. Agrawal, *Physica E*, 2006, **33**, 249–262.

63 K. Raghavachari and V. Logovinsky, *Phys. Rev. Lett.*, 1985, **55**, 2853–2856.

64 K. Raghavachari, *Abstr. Pap. Am. Chem. Soc.*, 1986, **192**, 96.

65 K. Raghavachari, *J. Chem. Phys.*, 1986, **84**, 5672–5686.

66 S. Li, R. J. Vanzee, W. Weltner and K. Raghavachari, *Chem. Phys. Lett.*, 1995, **243**, 275–280.

67 A. D. Zdetsis, *J. Chem. Phys.*, 2007, **127**, 014314.

68 P. Karamanis, D. Zhang-Negrerie and C. Pouchan, *Chem. Phys.*, 2007, **331**, 417–426.

69 E. C. Honea, A. Ogura, C. A. Murray, K. Raghavachari, W. O. Sprenger, M. F. Jarrold and W. L. Brown, *Nature*, 1993, **366**, 42–44.

70 K. Raghavachari and C. M. Rohlfing, *J. Chem. Phys.*, 1988, **89**, 2219–2234.

71 G. Meloni and K. A. Gingerich, *J. Chem. Phys.*, 2001, **115**, 5470.

72 B. W. Ticknor and M. A. Duncan, *Chem. Phys. Lett.*, 2005, **405**, 214–219.

73 M. Pellarin, C. Ray, P. Melinon, J. Lerme, J. L. Vialle, P. Keghelian, A. Perez and M. Broyer, *Chem. Phys. Lett.*, 1997, **277**, 96–104.

18970 | *Phys. Chem. Chem. Phys.*, 2015, **17**, 18961–18970

This journal is © the Owner Societies 2015